MEGA JOURNAL OF CASE REPORTS

OPEN ACCESS

Research Article

Compiled Date: September 18, 2025

High- Sensitivity Diamond-tipped Thermal Sensor for Non-Invasive Skin Cancer Detection: Development and Validation – Part B

Nathalie Nick[1*], Joe Kirkup[1], Parv Sains[2] and Kam Chana[1]

[1]University of Oxford, Department of Engineering Science, Parks Road, Oxford, OX13PJ, UK

[2]SainsSurgical. 4 Elsworthy, Thames Ditton, Surrey, KT7 0YP

[*]**Corresponding author**: Nathalie Nick, University of Oxford, Department of Engineering Science, Oxford, OX13PJ, UK

Abstract

This study reports experimental validation of a high-sensitivity diamond-tipped thermal product sensor for non-invasive skin cancer detection, complementing the design and modelling presented in Part A of this paper. Calibration with air and water confirmed baseline sensitivity improvements of an order of magnitude compared with previous thin-film based thermal product sensors. Accuracy of the measurement system was established through glycerol validation, while repeatability studies across multiple sessions yielded coefficients of variation <1%. Measurement uncertainty analysis showed combined uncertainties of 0.16-0.32°C in the temperature measurement and 0.26 in the thermal product evaluation. This comfortably exceeds diagnostic detection thresholds. Predictive modelling with interval PLS demonstrated excellent generalisation and linearity (RMSECV = 17.86 J/(m^2 K s$^{0.5}$); R^2 = 0.999), further validated against blind samples. Preliminary porcine testing confirmed clear differentiation of skin, fat, muscle, and fascia. Together, these results validate the robustness and demonstrate clinical potential of diamond-tipped thermal sensors as a development for real-time, non-invasive cancer diagnostics.

Keywords: Thermal product sensor; Diamond substrate; Skin cancer detection; Non-invasive diagnostics; Thermal properties; Biomedical sensing

Introduction

Accurate, early detection of skin cancer is critical for patient outcomes and healthcare efficiency. Current approaches depend on visual inspection and invasive biopsy, with high costs and unnecessary excisions [1-3]. Thermal product sensing has emerged as a promising technique for tissue characterisation, with thin-film sensors previously demonstrating proof-of-concept discrimination of malignant/benign lesions, being extensively thermally modelled, and showing potential for

integration with machine learning [4-6]. However, limitations including low sensitivity, fragile design, and electrical safety concerns limit their clinical approval. Part A of this study presented a novel diamond-tipped sensor design that leverages the exceptional thermal properties of single crystal diamond to overcome all these limitations. This paper (Part B) focuses on the experimental validation of the new sensor concept. Calibration with reference materials was performed to establish sensitivity, glycerol validation confirms quantitative accuracy, repeatability and uncertainty analysis demonstrate robustness and clinical suitability. A predictive statistical model is developed and validated against blind samples, and preliminary porcine testing illustrates biological tissue discrimination. These results demonstrate the feasibility of the diamond sensor as a robust, routine clinical diagnostic tool.

Experimental Validation

Material Testing Protocol

Performance validation of the diamond-tipped thermal sensor was conducted with a series of controlled bench top experiments. The probe consisted of a 2 mm diameter, 1 mm thick single-crystal diamond substrate bonded to a polyimide pedestal and housed within a stainless steel probe body **(Figure 1).** Heating was applied via a fine-wire element placed at the rear of the diamond, and temperature was measured using a fast response K-type thermocouple which was brazed to the rear of the diamond, with signal conditioning provided by dedicated electronics.

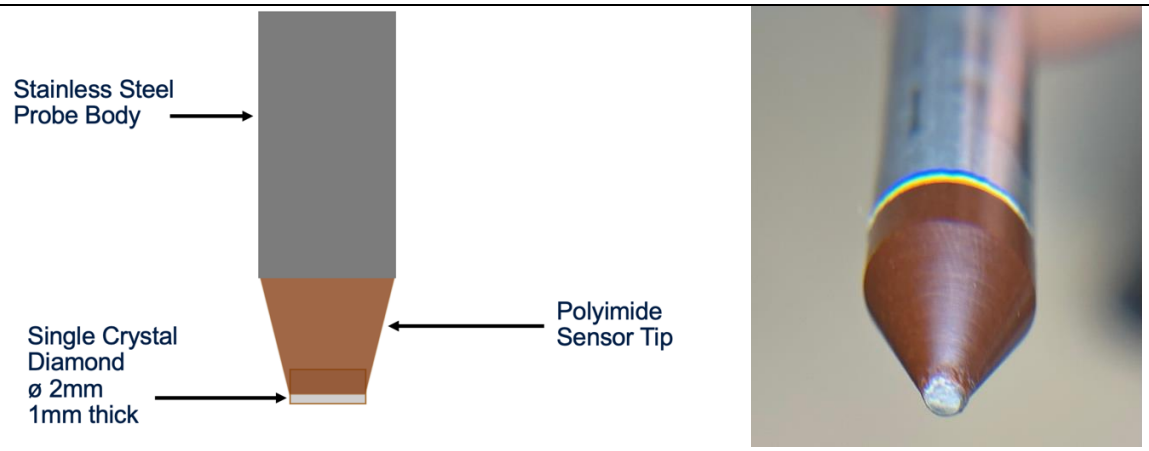

Figure 1: Sensor schematic (left) and manufactured probe (right).

Testing was conducted on air, purified water, and glycerol; chosen to span a wide range of thermal product values **(Table 1).** This range covers differences comparable in magnitude to those reported between normal and cancerous human skin ($\Delta TP \approx 380$ J/(m^2 K s$^{0.5}$)), thereby providing a clinically relevant benchmark. For each material, measurements were performed under controlled heating and measurement conditions to ensure comparability.

Table 1: Tested materials for validation.

Material	Density [kg/m³]	Specific Heat [J/kg·K]	Thermal Conductivity [W/m·K]	Thermal Product [J/(m² K s^0.5)]
Air	1.225	1006	0.026	6
Glycerol	1250	2380	0.286	922
Purified Water	997.049	4181.5	0.607	1591

Results

Sensor Calibration with Air and Water

Experimental calibration is presented in **Table 2,** where air and purified water is used to demonstrate the enhanced sensitivity compared to previous thin film probes. Results show an improvement of 12.6x and 5.2x for the sensors tested. The difference in manufacture between the two sensors lies in the thermocouple bonding method to the rear of the single crystal diamond disc.

Table 2: Diamond Sensor Performance with Air and Water Reference Materials

Sensor name	Power run at [W]	Max. Measured ΔT Air-Water [°C]	Time when Max. Measured ΔT Air-Water [s]	TP Difference Air (6) - Water (1582) (ΔTP = 1576 [J/(m² K s^0.5)])	Sensor Sensitivity TP/ΔT [°C/TP]	Sensitivity Improvement compared to thin film gauge sensor
G-1-Dev-001 (Brazed Thermocouple)	2.9	20.63	4.63	1576	0.013090	x12.62
G-1-Dev-002 (Adhesive Bonded Thermocouple)	9.38	8.49	1.39	1576	0.005384	x5.20

Figure 2 shows the temporal temperature response for both air and water measurements using sensor G-1-Dev-001 run at 2.9W for 1 second. The maximum temperature difference of 20.63°C was achieved at 4.63 seconds, corresponding to a sensor sensitivity of 0.013090°C/TP.

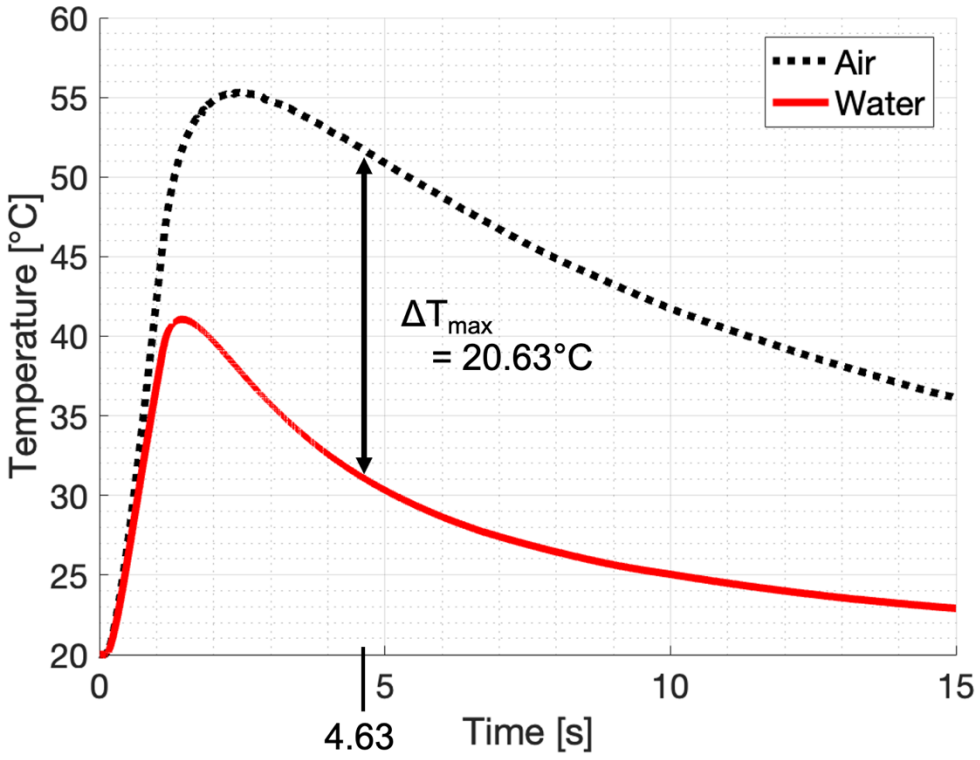

Figure 2: Maximum air-water temperature difference of 20.63°C. This represents a sensor sensitivity of 0.013090 °C/TP

The diamond sensor power requirement has been reduced and demonstrated good thermal coupling between the substrate and test material. The improved coupling provided by the 2 mm single crystal diamond disc with the test material enables the order of magnitude greater sensitivity.

Sensor validation using Glycerol

Figure 3 depicts the temperature measurement results of air, water and glycerol, with a heat pulse input of 0.25 seconds at 9.38W using the sensor G-1-Dev-002.

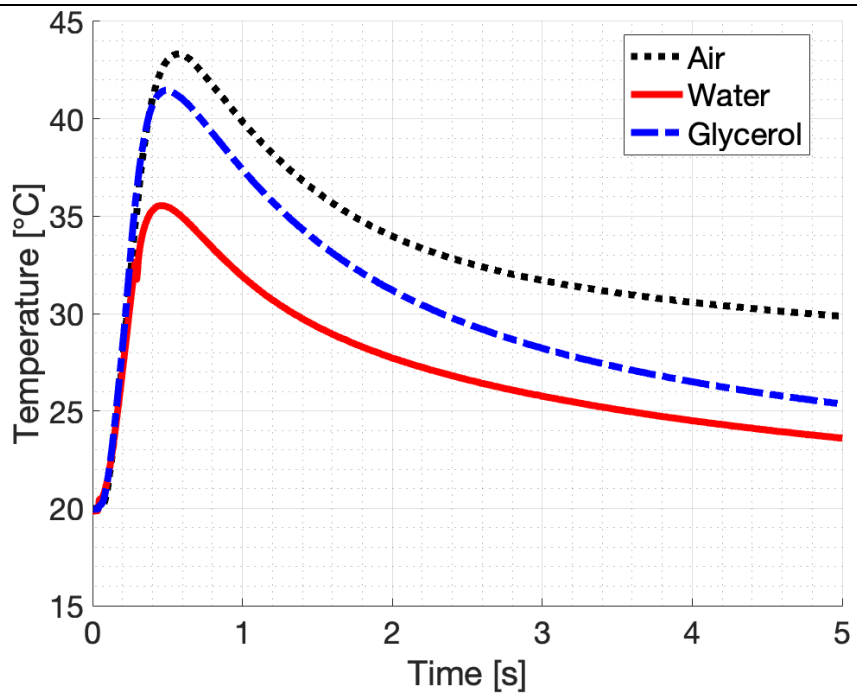

Figure 3: Temperature response of sensor G-1-Dev-002 to air, water, and glycerol.

To determine the thermal product of glycerol, linear interpolation was performed using air and water due to their precise thermal product characterisation in the literature. The evaluated thermal product value of glycerol was 912.7 J/(m^2 K $s^{0.5}$) with an uncertainty of ±0.5%, while the open literature reports a value of 922 J/(m^2 K $s^{0.5}$) with an uncertainty of ±2.5%. This method demonstrates the exceptional accuracy achieved, validating the sensors quantitative capability.

All measurements were corrected for ambient temperature changes to a common baseline of 20°C, with a 0.25-second heat pulse at 9.38W power input, ensuring temperatures remained below the 42°C dermatological safety threshold. The demonstrated accuracy for glycerol is particularly relevant as this value falls within the range given for human skin legions by DeGiovanni **[6].**

Repeatability and Statistical Analysis

To assess measurement precision, repeatability analysis was conducted using 10 independent measurements of each reference material using the sensor G-1-Dev-002.

Figure 4 presents the temperature measurement results of purified water. The temperature differences between the 10 different measurements lie between approximately ±0.05°C during the temperature decay once the peak is passed. The peak shows a slightly larger difference due to the data digitisation bandwidth not always capturing the peak location accurately.

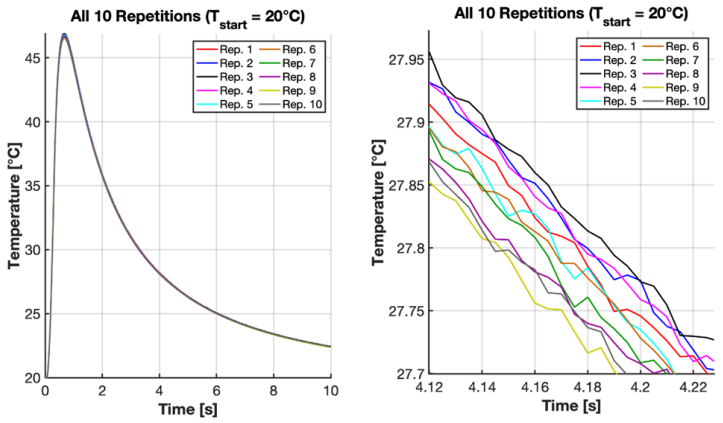

Figure 4: Temperature measurement results of purified water (left), with a magnified window at 4.12-4.22 seconds showing a temperature range of ~0.1°C (right).

Multiple measurement sessions demonstrated consistent precision, with water measurements achieving Coefficient of Variation (CV) values ranging from 0.25% to 0.85% across different sessions, glycerol showing CV of 0.35%, and air demonstrating CV of 0.46%. The 95% confidence intervals for the mean responses ranged from ±0.073°C to ±0.190°C across all materials and sessions, confirming high measurement precision. A summary of the CV and confidence limits is given in **Table 3** below for 10 repeats of each material.

Table 3: Repeatability Analysis Summary (n=10 each material)

Material	CV [%]	95% CI [°C]
Air	0.46	±0.123
Glycerol	0.35	±0.089
Water (Session 1)	0.85	±0.190
Water (Session 2)	0.25	±0.073

CV < 2% indicates excellent repeatability for clinical instruments.

Key Observations

Material Discrimination: The sensor successfully discriminated between all three materials with statistically significant differences across multiple measurement sessions.

Exceptional Precision: All materials achieved CV < 1% for maximum temperature, with the best water session reaching CV = 0.25%, representing outstanding precision that significantly exceeds clinical instrument requirements (typically CV < 5%).

Session Consistency: Multiple measurement sessions demonstrated reproducible performance, with water measurements showing CV range of 0.25-0.85%, confirming robust sensor operation across different experimental conditions.

Measurement Uncertainty and Error Analysis

An uncertainty analysis was performed to assess the sensor's clinical suitability by identifying and quantifying all significant error sources. The total measurement uncertainty was calculated using the root-sum-of-squares method, combining random (Type A) and systematic (Type B) uncertainty components. The analysis incorporated data from multiple measurement sessions to provide

conservative uncertainty estimates. The dominant uncertainty source was measurement repeatability, with session-dependent contributions ranging from ±0.12°C to ±0.31°C for water measurements. Additional systematic uncertainties included thermocouple calibration (±0.05°C), thermal contact variations (±0.05°C), environmental effects (±0.03°C), and baseline correction (±0.02°C). Digital quantisation and electrical noise contributed negligibly (±0.014°C combined).

Using the most conservative repeatability data, the total combined measurement uncertainties were ±0.32°C for water, ±0.22°C for air, and ±0.16°C for glycerol, corresponding to relative uncertainties of 0.89%, 0.50%, and 0.39% respectively. However, optimal measurement conditions achieved uncertainties as low as ±0.14°C for water, demonstrating the sensor precision potential**. Table 4** summarises the measurement uncertainty in temperature measurement translated to thermal product.

Table 4: Measurement Uncertainty Budget.

Error Source	**Air**	**Water**	**Glycerol**	**Type**
Repeatability [°C]	±0.200	±0.310*	±0.140	Random
Calibration [°C]	±0.050	±0.050	±0.050	Systematic
Environmental [°C]	±0.030	±0.030	±0.030	Systematic
Thermal Contact [°C]	±0.050	±0.050	±0.050	Systematic
RSS Total [°C]	**±0.216**	**±0.320**	**±0.162**	**Combined**
TP Uncertainty [J/(m^2 K s$^{0.5}$)**]**	**6±0.001**	**1591±0.23**	**922±0.26**	**Combined**

**Conservative estimate; optimal conditions achieve ±0.118°C*

Under conservative conditions, where the uncertainty for water is ±0.23TP units, and air is ±0.01 TP units the maximum predicted uncertainty of an unknown sample will be ±0.231 TP units. This correlates reasonably well with the measured measurement uncertainty given in **Figure 4** (right) of ±0.05°C.

In clinical and analytical contexts, the sensor meets stringent clinical requirements with temperature uncertainties well below 0.32°C thresholds and relative uncertainties <0.26 TP units. A minimum SNR of around 3:1 is typically considered sufficient to ensure reliable detection, while an SNR of 10:1 is generally required for precise quantification, as outlined in analytical method validation guidelines (e.g., ICH Q2(R2)) **[7].** For the present application, which focuses on distinguishing between cancerous and normal skin rather than precise quantification, the 3:1 criterion is most relevant. The sensor SNR is ~54:1 at 27°C thus exceeding this threshold, with optimal conditions even approaching/surpassing the stricter quantification criterion, providing strong confidence for clinical skin cancer detection.

Predictive Modelling and Blind Sample Validation

To extend beyond direct calibration and uncertainty analysis, a predictive statistical model was developed to generalise sensor responses to unknown samples. This section describes the data pre-processing, interval partial least squares (iPLS) modelling, and blind sample validation used to evaluate the robustness and predictive capability of the sensor. Temperature profiles were imported into MATLAB R2022a (Mathworks) for initial inspection and clean-up, with sampling discontinuities addressed by mean-averaging the adjacent variables. Normalisation of the data was also performed by mean-averaging the initial 10 "pre-pulse" variables and subtracting this value from all variables, producing a "delta temperature" measurement where initial temperature offset as a result of environmental factors was eliminated to minimise baseline variation. Any raw or averaged data figures and performance metrics such as standard deviations were also produced at this stage.

The processed data was exported from MATLAB and imported to Solo 9.1 (Eigenvector Research Inc.) for the creation of the primary statistical model. An interval partial least squares (iPLS) model was initially created: "X and Y" matrix data were separated into their respective blocks in the model workflow before data pre-processing treatments were applied. A variable selection process via forward partial least squares was initiated, with a window width of 1 sample and the window number set to "auto". This variable selection process identified the time point t = 0.574-0.575 seconds as producing the lowest Relative Mean Squared Error of Cross-Validation (RMSECV) which can be seen in **Figure 5.**

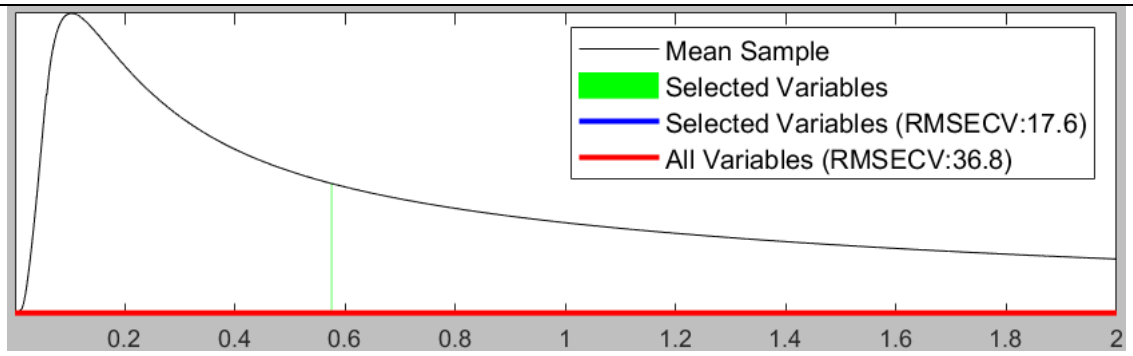

Figure 5: The variable time point identified via the forward PLS algorithm as giving rise to the greatest variation in the tested samples.

Use of such a narrow band compared to the overall variable width indicates (before the model is even constructed) that the X/Y relationship is likely to be simple/linear with low dimensionality. A cross-validation scheme of "Venetian blind" was selected with n = 6. Model statistics such as RMSECV (Root Mean Squared Error of Cross-Validation) and R^2 (coefficient of determination) were calculated. Solo model optimiser was utilised at this stage to perform a parametric study – sweeping all reasonable permutations – to obtain the model with the lowest RMSECV. This included altering the fundamental model type between Principal Component Regression (PCR), PLS, and Support Vector Regression (SVR); and the model parameters such as pre-processing and window width for variable selection. Blind samples were then loaded into the model for comparison with the training data and the "predicted concentration vs. actual concentration" plots generated.

Statistical Model Results

Figure 6 shows the nominal thermal product for each sample plotted against the thermal product predicted by the model, with the theoretically "perfect 1:1 line" in green and the "actual model line" in red.

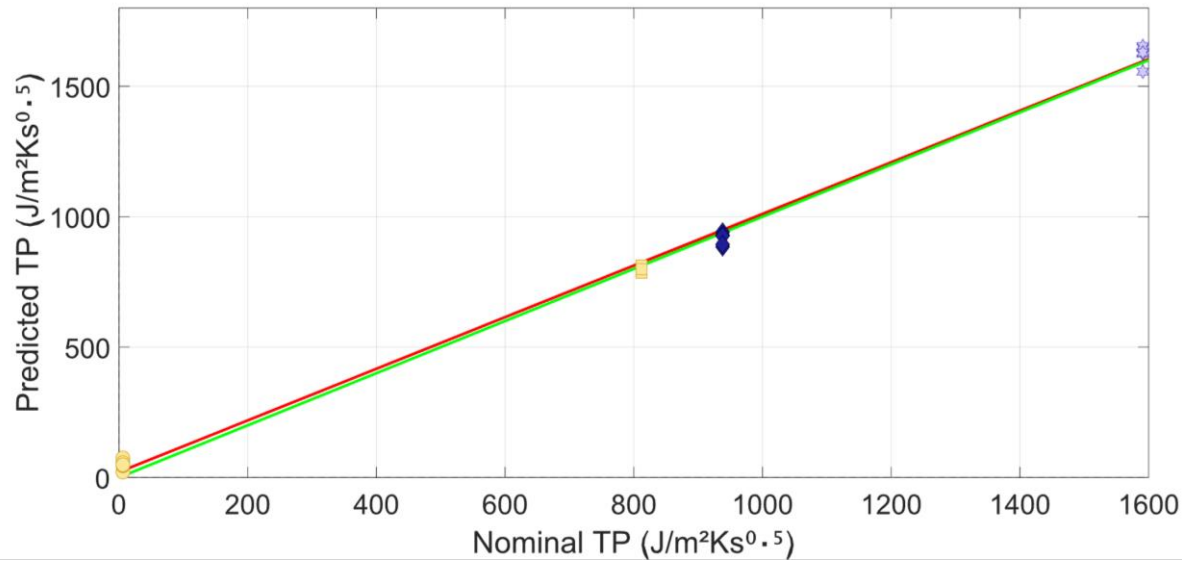

Figure 6: Nominal thermal product vs. predicted thermal product via the iPLS model.

The model demonstrates excellent predictive capabilities with an RMSEC = 16.51 J/(m^2 K $s^{0.5}$) and an RMSECV = 17.86 J/(m^2 K $s^{0.5}$). Therefore, the model should generalise other samples with thermal products in a similar region to the training data; with samples in regions such as 100-600 J/(m^2 K $s^{0.5}$) needing additional testing for full validation. R^2C and R^2CV were both 0.999 (3 d.p.) indicating strong linearity in the model.

A set of four blind samples were processed based on the above model, further confirming the robustness of the predictive model, the results of which are detailed in **Table 5.**

Table 5: Results of processed samples.

Samples #	Nominal TP (J/(m^2 K $s^{0.5}$))	Predicted TP (J/(m^2 K $s^{0.5}$))	Error From Nominal (%)
1	812.0	819.5	0.9
2	938.0	914.5	2.5
3	1591	1590.0	0.1
4	1591	1594.4	0.2

The predicted thermal product values were in close agreement with their nominal counterparts, with errors ranging from 0.1% to 2.5%. Most samples exhibited less than 1% deviation, demonstrating strong consistency across different thermal product values. Even for the Sample 2 outlier, the error remained within an acceptable range, suggesting the model is reliable for practical application. There may also be a larger uncertainty in the nominal TP value for sample 2, increasing the actual accuracy of the model further. Overall, the blind test

highlights the strong generalisation capability of the model within the tested region.

Preliminary Porcine Testing

Preliminary ex-vivo measurements were performed on porcine belly tissue using the diamond-tipped sensor G-1-Dev-001 prior to extensive biological tissue testing. Four distinct tissue types skin, fat, muscle, and fascia were characterised – with 2.9W over a time span of 1 second being applied to all samples. The experimental setup is shown in **Figure 7.**

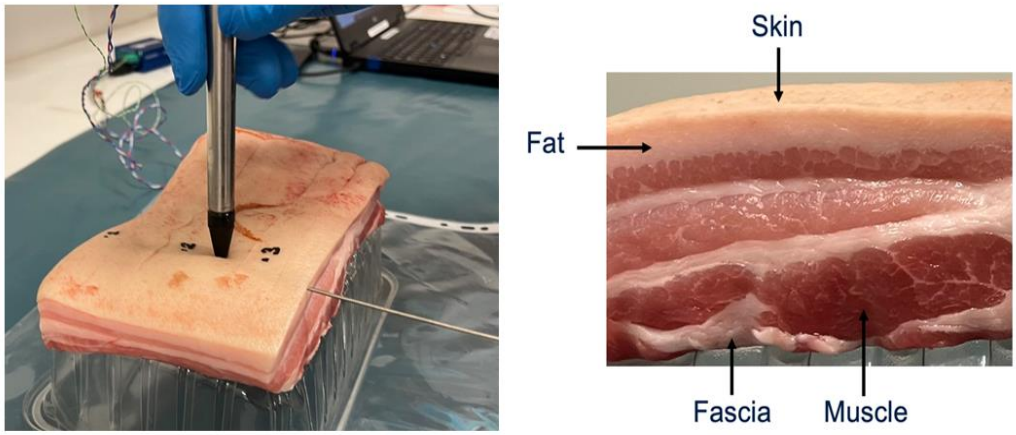

a) Experimental setup

b) Measured layers: skin, subcutaneous fat, muscle and fascia

Figure 7: Preliminary porcine testing using the novel diamond-based thermal sensor G-1-Dev-001.

The experimental results are shown in **Figure 8**. Clear differentiation between tissue types was observed, consistent with their expected different thermal product values, the curves showing the different values of thermal product for each layer. These findings provide an initial indication that the sensor can clearly discriminate between different biological tissues, and they align with trends reported in previous studies using earlier thin-film sensors. Further analysis and systematic validation are carried out and will be the subject of the next paper.

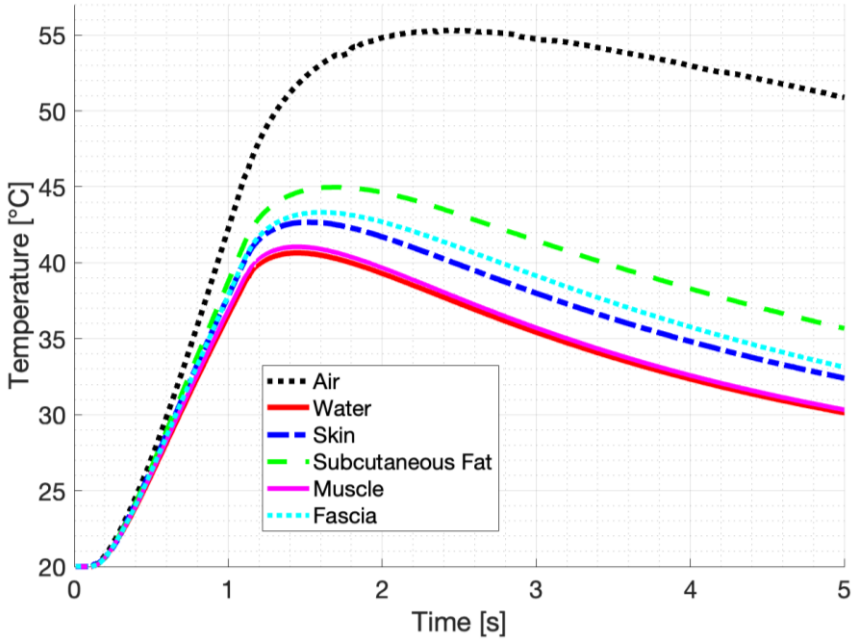

Figure 8: Measured temperature response of porcine skin, subcutaneous fat, muscle and fascia. Air and distilled water for calibration.

This dataset was used to calculate the thermal product of porcine tissues by establishing a linear calibration between air (TPair = 6) and water (TP_{water} = 1582). Using this relationship (0.013090 °C/TP), the thermal product values were determined as follows: TP_{skin} = 1395, TP_{fat} = 1140, TP_{muscle} = 1559, TP_{fascia} = 1327. These values are consistent with previously reported measurements, with expected variations attributable to the ex-vivo conditions (frozen storage, absence of perfusion). The results support the feasibility of the sensor for differentiating soft tissues and motivate further work on in-vivo testing.

Discussion

The experimental validation confirms the performance improvements predicted in Part A. Calibration with air and water demonstrated sensitivities of 0.013090°C/TP, representing 12.6-fold improvements over thin-film based thermal product probes **[6,8].** Glycerol interpolation yielded a 1.01% error against an open literature published value (published value error given as 2.5%), demonstrating quantitative capability across clinically relevant thermal product ranges. Repeatability analysis across multiple sessions showed coefficients of variation below 1% for all materials, substantially better than the <5% CV typically required for clinical instruments. Measurement uncertainties were conservatively estimated at ±0.32°C for water, corresponding to ±0.23 J/(m^2 K $s^{0.5}$) in thermal product. These uncertainties translate to signal-to-noise ratio of 54:1 at 27°C for distinguishing normal from cancerous skin ($\Delta TP \approx 380$ J/(m^2 K $s^{0.5}$)), comfortably exceeding the 3:1 minimum typically required for reliable clinical detection **[7].**

Predictive modelling with iPLS confirmed strong generalisability (R^2 = 0.999), with blind sample errors of 0.1–2.5%. This demonstrates the robustness of the approach and its potential for application to unknown samples. Preliminary porcine testing further supports biological relevance, showing clear discrimination of skin, fat, muscle, and fascia. These results align with previous thin-film sensor studies **[4,8]** but demonstrate substantially improved sensitivity and robustness.

Current diagnostic practice relies on visual inspection with accuracies of 60–80%, followed by invasive biopsy as the gold standard. The present sensor demonstrates the potential to achieve >95% discrimination accuracy based on thermal product differences, with sub-second measurement times. Future work will focus on systematic biological tissue validation, standardisation of measurement protocols, and in vivo clinical trials.

Conclusions

Experimental validation confirmed the diamond-tipped sensor demonstrated enhanced performance, achieving 12.6-fold sensitivity gains, <1% repeatability error, and SNR values well above the 3:1 clinical threshold. Blind sample validation and preliminary porcine testing demonstrated robust material and tissue discrimination. Together, these results highlight the strong clinical promise of diamond-tipped thermal based sensing for rapid, non-invasive skin cancer detection.

Acknowledgements

The authors acknowledge Principal Technologies Inc. for funding the skin cancer research.

Dr Santonu Ghosh from Element Six UK Ltd. is acknowledged for the assistance provided for the diamond materials. Sunny Chana and Jamie Dean from Oxford University are acknowledged for their contributions for the manufacturing of the sensor parts.

References

1. Cancer Research UK. Melanoma skin cancer statistics. 2024.
2. Ethna McFerran et al. "Skin in the game: The cost consequences of skin cancer diagnosis, treatment and care in Northern Ireland". J Cancer Policy. 2024:39:100468.
3. NHS England. National Cost Collection for the NHS. Reference Costs. 2024.
4. Nick N, et al. "Thermal Product Sensing: Simulations and Experiments of a Novel Biosensor for Quantitative Thermal Property Measurement of Biological Tissues". Mega J Case Rep. 2025;8(6):2001-2019.
5. Nick N, et al. "Machine Learning Classification of Skin Lesions Using Thermal Product Biosensing: A Preliminary Diagnostic Approach". Mega J Case Rep. 2025;8(6):2001-2011.
6. DeGiovanni C, et al. "Thermal Product Sensor: A potentially new diagnostic tool in the detection of skin malignancy". Medical Research Archives. 2024.
7. Committee for Medicinal Products for Human Use. ICH guideline Q2(R2) on validation of analytical procedures. 2022.
8. P Sains, KS Chana, V Sridhar, MS. Sajid. Pilot study on an innovative biosensor with a range of medical and surgical applications. BMC Res Notes. 2018;11(1):81.

Citation of this Article

Nick N, Kirkup J, Sains P and Chana K. High- Sensitivity Diamond-tipped Thermal Sensor for Non-Invasive Skin Cancer Detection: Development and Validation – Part B. Mega J Case Rep. 2025;8(9):2001-2012.